


Controllable quantum walks, gravitational constant, and Casimir energy in one-dimensional three-boson systems with on-site interactions

Hongting Yang* and Pinquan Qin 

School of Science, Wuhan University of Technology, Wuhan 430070, China



(Received 18 November 2023; revised 22 June 2024; accepted 24 June 2024; published 3 July 2024)

This study scrutinizes one-dimensional three-boson systems with on-site interactions, delving into perturbation theory, continuous-time quantum walks, and quantum Fisher information (QFI), among other areas. Notably, two critical on-site interaction strength points emerge. At these specific locations, the QFI reaches its zenith, exhibiting a proportionality to t^4 . This substantively amplifies the precision in measuring both the Newtonian constant of gravitation and the Eötvös parameter. The improvement surpasses models devoid of on-site interactions by 6 orders of magnitude. The methodology used to measure big G can be adapted to quantify the Casimir energy of a many-particle system.

DOI: [10.1103/PhysRevB.110.014302](https://doi.org/10.1103/PhysRevB.110.014302)

I. INTRODUCTION

Quantum walks [1,2], often considered as the quantum counterpart of classical random walks, have garnered significant interest in various fields, including quantum algorithms [3,4], quantum simulation [5–8], quantum information [9,10], quantum computation [11], and even quantum biology [12,13]. In the realm of quantum walks, studies on Anderson localization [14], topological phases [15–20], and magnon bound states [21–24] have attracted considerable attention. These quantum walks involve various types of walking particles, including specific atoms [25–27], ions [28–30], photons [31–37], and more general indistinguishable particles, such as bosons, fermions, and anyons [38–51]. Furthermore, quantum systems under the influence of electric or magnetic fields [52–55] or gravity [56–59] have provided valuable insights. Precision measurements in gravitational quantum walks are a particularly intriguing area of research [60–62]. Concurrently, efforts persist in the measurement of the Newton constant of gravitation and the examination of the Einstein equivalence principle. A recent atom-interferometric measurement has pushed the precision of the Eötvös parameter to the 10^{-12} level [63], while advancements in the precision of gravitational constant measurements over the last two centuries amount to an improvement of merely about 2 orders of magnitude [64].

The research conducted in 2015 presented insights into quantum walks and Bloch oscillations involving two bosons with on-site interaction in optical lattices [65]. A recent study in 2021 focused on many-particle quantum walks and Fisher information in one-dimensional lattices, demonstrating bunching or antibunching behavior, Bloch oscillations, and time scaling of the quantum Fisher information (QFI) in a system of three indistinguishable particles with nearest-neighbor interaction [66]. It is important to note that this study did not include on-site interaction. Additionally, research on quantum

walks involving three bosons in a one-dimensional lattice has been carried out, considering two- and three-body interactions [67]. Our research aims to study quantum walks and QFI of three bosons in the one-dimensional Bose-Hubbard model. The Bose-Hubbard model is a fundamental theoretical framework for understanding the behavior of ultracold atoms in optical lattices and is widely used in quantum physics research. These studies shed light on the intriguing dynamics of quantum systems, particularly in the context of Bose-Hubbard models and quantum walks, and provide valuable insights for further research in quantum information theory and quantum computing.

The treatment of quantum many-body systems poses a substantial challenge due to the exponential growth of the Hilbert space with system size, even in the case of relatively small systems. In recent decades, various methods have been developed to effectively calculate the time-evolution operator in large Hilbert spaces constructed using matrix product states (MPS) [68]. Some of the well-established approaches include:

- (i) Time-evolving block decimation (TEBD) and other density matrix renormalization group (DMRG) schemes [69–73];
- (ii) The matrix product operator (MPO) method, denoted as $W^{1,II}$ [74];
- (iii) The Krylov method, which incorporates the Lanczos process, the variational approach, and other computational techniques [75–77]; and
- (iv) The time-dependent variational principle (TDVP) [78,79].

The choice of method depends on the specific requirements of the study and the system being analyzed. To study the dynamics and Bloch oscillations of a one-dimensional three-boson system with on-site interaction, the Krylov method is employed. The continuous-time evolution method is utilized, allowing the application of the evolution operator at any time, in contrast to the discrete-time evolution method, where it is applied at discrete time steps [3,9,80].

*Contact author: yht@whut.edu.cn

The research focuses on obtaining the energy spectrum, analyzing its structure, and applying perturbation theory to understand the system's behavior under strong on-site interaction. The dynamics starting from the ground state reveal fermionlike behaviors in terms of density and density-density correlation. The study also explores Bloch oscillations, providing insight into the characteristic frequency of the three-boson system. Quantum Fisher information results guide experimentalists in selecting an appropriate value for on-site interaction.

II. THE BOSE-HUBBARD MODEL OF THREE PARTICLES WITH ON-SITE INTERACTION

The Bose-Hubbard model captures the behavior of ultracold bosonic atoms within a lattice. In this system, bosons can tunnel between lattice sites with a hopping strength represented by J , and they experience on-site interactions, either attractive or repulsive, denoted by the parameter U . This interaction energy depends on the number of bosons on each site, as given by the term $\sum_i \frac{U}{2} n_i(n_i - 1)$. Additionally, an external field introduces an energy shift per site, denoted as F . The Bose-Hubbard Hamiltonian represented by the equation

$$H = \sum_{(i,j)} J a_i^\dagger a_j + \sum_i \frac{U}{2} n_i(n_i - 1) + \sum_i iF n_i \quad (1)$$

combines these elements to describe the overall energy of the system. This Hamiltonian is a fundamental concept in the study of ultracold quantum gases and is widely used to understand the behavior of bosons in optical lattices.

The energy spectrum for a system without an external field is given as follows. The eigenstate $|\Psi\rangle$ of the model is governed by the Hamiltonian operator H , resulting in the Schrödinger equation $H|\Psi\rangle = E|\Psi\rangle$. The eigenenergy spectrum of the model can be obtained by the exact diagonalization method of the Hamiltonian [45], with the length of the lattice being $L = 21$. The Hamiltonian is 121×121 dimensional, consequently there are 121 values of eigenenergy for each value of k_i . For simplicity, we fix $J = 1$. The energy spectra of $U = 0.5, 1.8, 10.0$, and -10.0 are given in Fig. 1. At weak repulsion $U = 0.5$, there is only one band primarily composed of scattering states. The two-boson bound states (2BS) and three-boson bound states (3BS) are mixed with these scattering states. With increasing repulsion, 2BS and 3BS gradually emerge from the scattering states. At $U = 1.8$, the 3BS level becomes prominent. Strong repulsion $U = 10.0$ leads to the isolation of the 3BS band around energy $3U$ and the 2BS band around energy U from the scattering state band. As seen in the bottom right panel of Fig. 1, changing the interaction from repulsive $U = 10.0$ to attractive $U = -10.0$ shifts the 2BS and 3BS bands to the other side of the scattering state band, while the latter remains unchanged. This analysis provides insights into how local on-site interactions affect the energy spectrum of the Bose-Hubbard model with three bosons. The energy spectrum of this boson system resembles that of a one-dimensional three-fermion system with nearest-neighbor interaction.

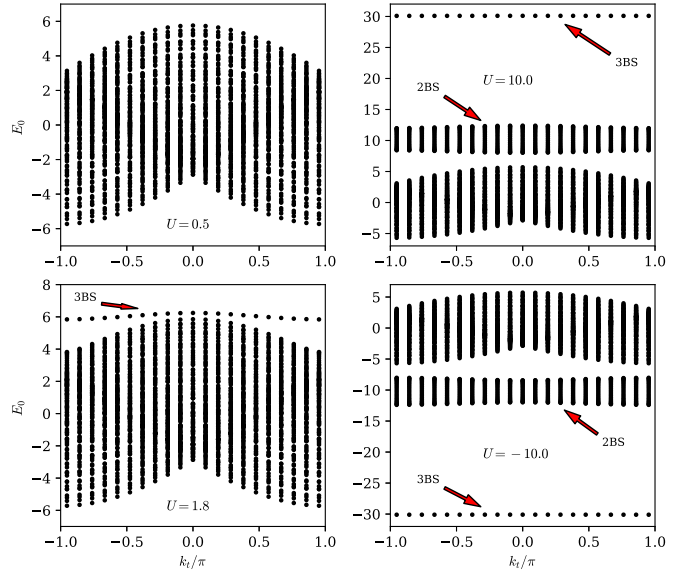


FIG. 1. The energy E_0 as a function of the total momentum k_i (in units of π) for different values of on-site interaction strength.

III. THE EFFECTIVE BOSE-HUBBARD MODEL AND THE DYNAMICS

In the regime of strong on-site interaction, it is anticipated that three bosons residing on the same lattice site will effectively merge, behaving as a single composite particle. To understand this phenomenon, perturbation calculations are employed to derive the effective single-particle Bose-Hubbard model. In this analysis, external forces are disregarded.

The Hamiltonian, denoted as H , is decomposed into two components: $H = H_0 + H_1$. Here, H_0 represents the on-site attraction part and is considered the unperturbed term, while H_1 stands for the hopping term and is treated as a perturbation. H_0 exhibits three distinct eigenvalues:

- (i) $E_0 = 3U$, corresponding to the ground state where three bosons occupy a single site, denoted as $\{|G_j\rangle = |j^3\rangle\}$;
- (ii) $E_1 = U$, associated with excited states where two bosons are bound together and the third boson is free, represented as $\{|E_{j_1 j_2}\rangle = |j_1^2 j_2\rangle\}$ with $j_1 \neq j_2$; and
- (iii) $E_2 = 0$, characterizing excited states where no bosons are bound together, expressed as $\{|E_{j_1 j_2 j_3}\rangle = |j_1 j_2 j_3\rangle\}$, with $j_1 < j_2 < j_3$.

In this context, $|j^n\rangle$ signifies n bosons, and $|j\rangle$ represents a single boson residing on site j . The many-body perturbation approach uncovers important insights into the behavior of a system in the limit of strong on-site interactions, where three bosons effectively merge into a single composite particle. By introducing projection operators derived from these states and applying many-body perturbation theory [45,66,81], the effective Hamiltonian up to third-order perturbation takes the form

$$H_{\text{eff}} = J_{\text{eff}} \sum_{(i,j)} b_i^\dagger b_j + \mu_{\text{eff}} \sum_j b_j^\dagger b_j, \quad (2)$$

where the effective hopping strength $J_{\text{eff}} = 3J^3/2U^2$, the chemical potential $\mu_{\text{eff}} = 3(U + J^2/U)$, and b_j^\dagger and b_j

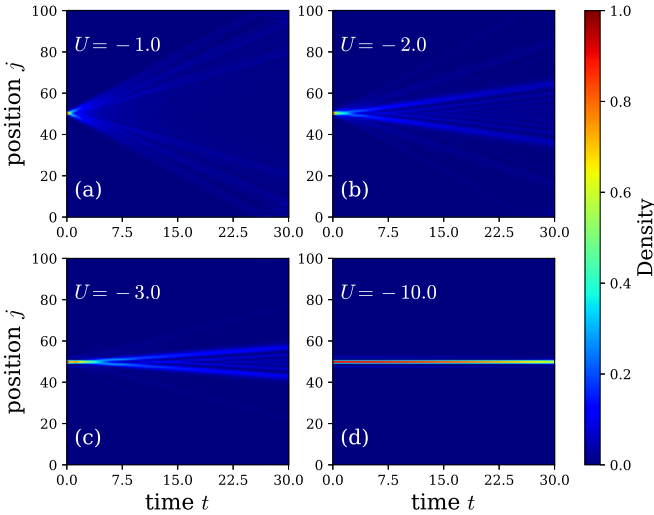


FIG. 2. Panels (a), (b), (c), and (d) display the time evolutions of particle density with increasing on-site interaction strengths, $U = -1.0, -2.0, -3.0$, and -10.0 , all commencing from the ground state $|G_j\rangle$, with $j = 50$.

represent the creation and annihilation operators for the composite particle consisting of three bosons on the j th lattice site. The quasiparticle spectrum of the effective Hamiltonian is obtained by substituting the ansatz $|\psi\rangle = \sum_m e^{ik_r m} b_m^\dagger |0\rangle$ into the equation $H_{\text{eff}}|\psi\rangle = E_{\text{eff}}|\psi\rangle$, which gives

$$E_{\text{eff}} = \frac{3J^3}{U^2} \cos k_t + 3\left(U + \frac{J^2}{U}\right), \quad (3)$$

with k_t representing the momentum of the quasiparticle. The resulting energy spectrum exhibits a characteristic single-particle behavior. In the time evolution dynamics, however, the quantum walks of this composite particle are significantly suppressed as the interaction strength U increases. It exhibits a maximal group speed of $v_{\text{max}} = 3J^3/U^2$. This behavior distinguishes it from the quasiparticle composed of two bosons with strong on-site interaction. For comparison, the energy of a quasiparticle composed of two bosons with strong on-site interaction is given by

$$E'_{\text{eff}} = \frac{4J^2}{U}(1 + \cos k_t) + U. \quad (4)$$

Given the wave function of the system $|\Psi(t)\rangle = e^{-iHt}|\Psi_0\rangle$, with $|\Psi_0\rangle$ as the initial state, the time evolution of the particle density $n_j(t) = \langle\Psi(t)|n_j|\Psi(t)\rangle$ is depicted in Fig. 2. In Fig. 2(a), there are three pairs of ballistic lines describing respectively the quantum walks of a single-particle state, 2BS, and 3BS. With increasing on-site interaction strengths, the innermost cone becomes brighter while the outer cones fade. In Fig. 2(d), only one bright horizontal line could be reached, which implies that the three bounded bosons tend to be static like a static particle without any external forces exerted on it. This behavior of three bounded bosons with strong on-site interaction is similar to the quantum walks of three fermions with strong nearest-neighbor interaction. In Fig. 3, the time evolution of particle density for $U = -2.0$ and $U = -3.0$ is revisited. The maximal group velocities, denoted as v_g , are

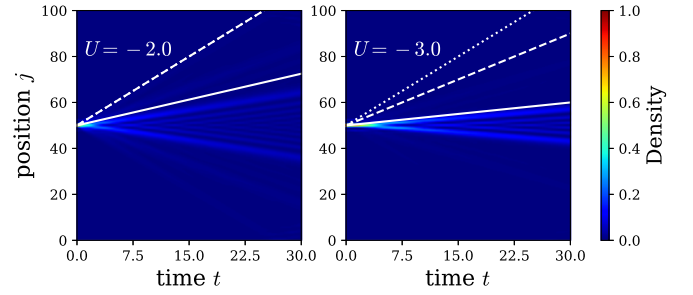


FIG. 3. The maximal group velocities of the quantum walks of the single-particle state (dotted line), 2BS (dashed line), and 3BS (solid line) are illustrated during the time evolution of particle density with varying on-site interaction strengths, specifically $U = -2.0$ and $U = -3.0$.

$2J$, $4J^2/|U|$, and $3J^3/U^2$ for the single-particle state, 2BS, and 3BS, respectively, initially positioned at site $j = 50$. For the case of $U = -2.0$, the dotted line aligns with the dashed line, given that $J = 1$ is constant. The values of the maximal group velocities for 2BS and 3BS exceed the slopes of the corresponding ballistic lines. In the case of $U = -3.0$, the maximal velocity of 3BS aligns well with the slope of the corresponding ballistic line, while the dynamic behaviors of the single-particle state and 2BS are too weak to be observed. The density-density correlations, denoted as $C(i, j) = \langle\Psi(t)|n_i n_j|\Psi(t)\rangle$, are displayed in Fig. 4. At $U = -1.0$, as time progresses, the co-walking of bosons along the diagonal becomes evident, alongside some independent off-diagonal walks of a single particle. As the on-site interaction strength increases, the phenomenon of antibunching diminishes, while the co-walking of three bosons exhibits slow movement. We do not discuss the case of $-U$, because the density is an even function in U when $F = 0$ [82], signifying that $n_j(t)|_U = n_j(t)|_{-U}$.

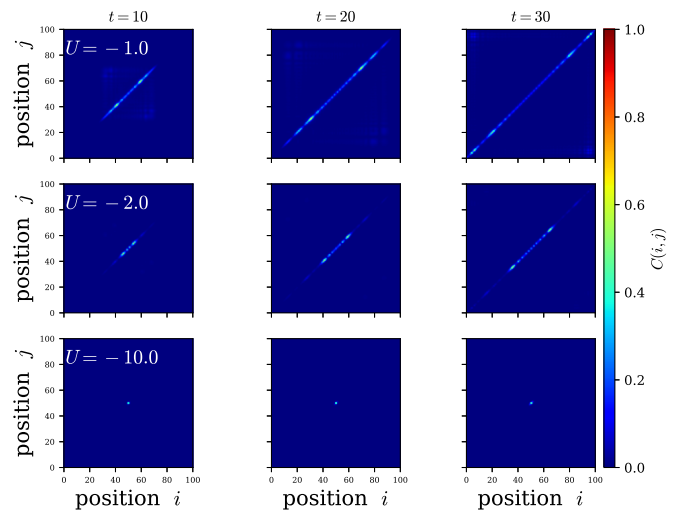


FIG. 4. The density-density correlations $C(i, j)$ with varying on-site interaction strengths $U = -1.0, -2.0$, and -10.0 and times $t = 10, 20$, and 30 .

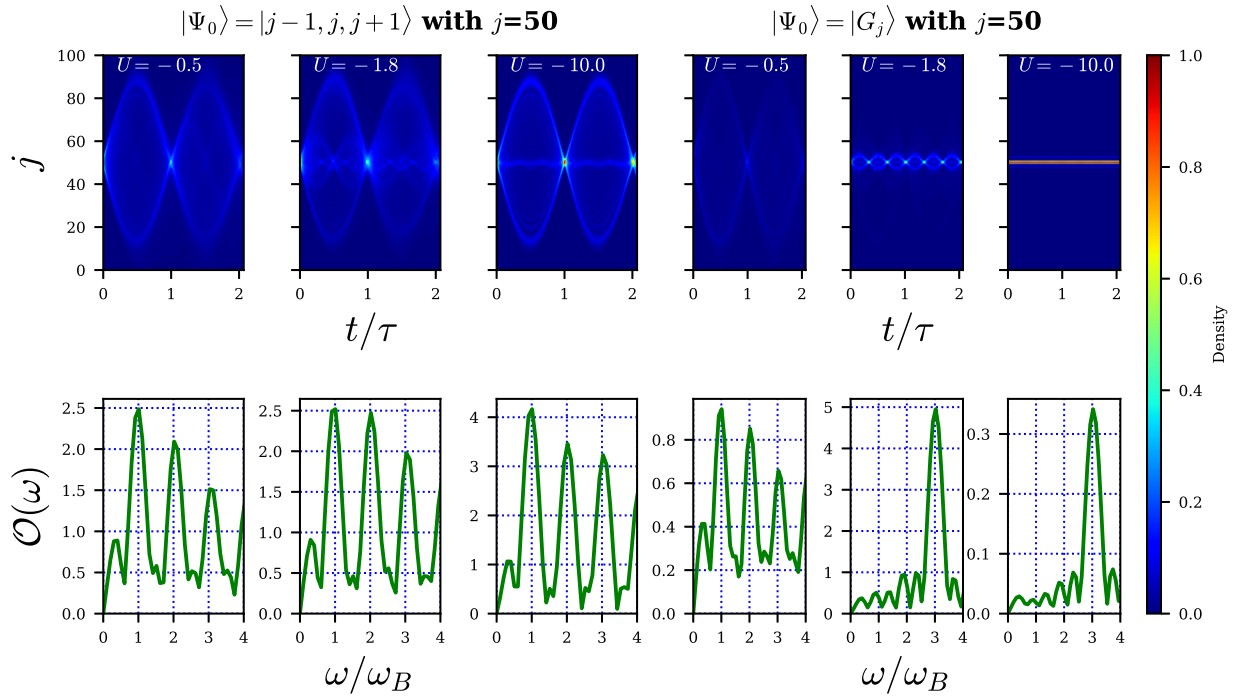


FIG. 5. The evolution of particle density starting from different initial states: $|\Psi_0\rangle = |j-1, j, j+1\rangle$ with $j = 50$ (left three columns) and $|\Psi_0\rangle = |G_j\rangle$ with $j = 50$ (right three columns), and the associated $\mathcal{O}(\omega)$ corresponding to $\mathcal{O}(t)$. The temporal period $\tau = 2\pi/\omega_B$, where angular frequency $\omega_B = F$, and $F = 0.1$ remains constant throughout the entire work.

IV. BLOCH OSCILLATION

The evolution of particle density with increasing on-site interaction and the associated discrete Fourier transform (DFT) $\mathcal{O}(\omega)$ of the density difference $\mathcal{O}(t) = \sum_j |n_j(t) - n_j(t=0)|/L$, when an external force F is applied, are depicted in Fig. 5. For the initial state $|\Psi_0\rangle = |j-1, j, j+1\rangle$ with $j = 50$, at $U = -1.8$, the evolutions of the single-particle state, 2BS, and 3BS are evident. However, for the other two cases, $U = -0.5$ and $U = -10.0$, only the evolution of the single-particle state is clear. Their DFTs in the lower left panels of this figure reveal angular frequencies of $\omega = \omega_B$, $2\omega_B$, and $3\omega_B$, and so on, with the abbreviation $\omega_B = F$. From the DFTs we can see that, with increasing on-site interaction, the intensity of the single-particle state is always the largest, followed the intensity by the 2BS, and the intensity of the 3BS is the smallest. In contrast, the dynamics of the three-fermion system with nearest-neighbor interaction (Fig. 4 of Ref. [66]) are evident. With increasing the nearest-neighbor interaction V , the intensity of the single-particle state, 2BS, and 3BS becomes the largest successively. If the evolution begins from the initial state $|\Psi_0\rangle = |G_j\rangle$ with $j = 50$, as U increases, the wave fronts of the single-particle state and 2BS fade away, resembling the evolution of a one-dimensional three-fermion system with nearest-neighbor interaction. However, the difference is that with increasing U , the DFT displays an early distinct peak with the angular frequency $3\omega_B$, implying that the 3BS is prominent when the evolution starts from the ground state with three bosons sitting on the same site. Further results on Bloch oscillation are discussed in the next section, focusing on the calculation of quantum Fisher information.

V. QUANTUM FISHER INFORMATION AND PRECISION MEASUREMENTS

We delve into the QFI, the reciprocal of the Cramér-Rao bound, in precision measurements related to gravitation. Originating from the evolution of a pure state $|\Psi_0\rangle$ through $|\Psi(t)\rangle = e^{-iHt}|\Psi_0\rangle$, the QFI is expressed as

$$Q = 4[\langle \partial_F \Psi(t) | \partial_F \Psi(t) \rangle - |\langle \Psi(t) | \partial_F \Psi(t) \rangle|^2]. \quad (5)$$

Here, the Hamiltonian H aligns with the form in Eq. (1). Introducing the operator function $h[x] = (e^x - 1)/x$, the adjoint operator $\text{ad}_H(A) = [H, A]$, and $G = h[\text{ad}_{iH}](\partial_F H)$, the QFI takes the form

$$Q = 4t^2(\langle \Psi_0 | G^2 | \Psi_0 \rangle - |\langle \Psi_0 | G | \Psi_0 \rangle|^2). \quad (6)$$

Incorporating the reduced Planck constant \hbar and the lattice spacing d , two critical values of U , $U = \pm Fd/2$, lead to maximum values of $Q = 3(Jd)^2(t/\hbar)^4$. The minimum relative uncertainty in measuring F is defined as

$$\left(\frac{\Delta F}{F}\right)_{\min} = \frac{\hbar^2}{d} \left(\frac{\Delta F}{F}\right)_0, \quad (7)$$

where the bare relative uncertainty $(\Delta F/F)_0 = 1/\sqrt{3}JFt^2$, allowing for deviations in actual calculations based on specific models and techniques. Notably, the Eötvös parameter $\eta = \Delta g/g$, and $\Delta G/G$, the relative uncertainty in measuring big G , equals to $\Delta F/F$: $\eta = \Delta g/g = \Delta G/G = \Delta F/F$.

If the on-site interaction vanishes, the QFI value $Q_0 = 24(Jt/\hbar F)^2$ leads to a relative uncertainty in measuring F

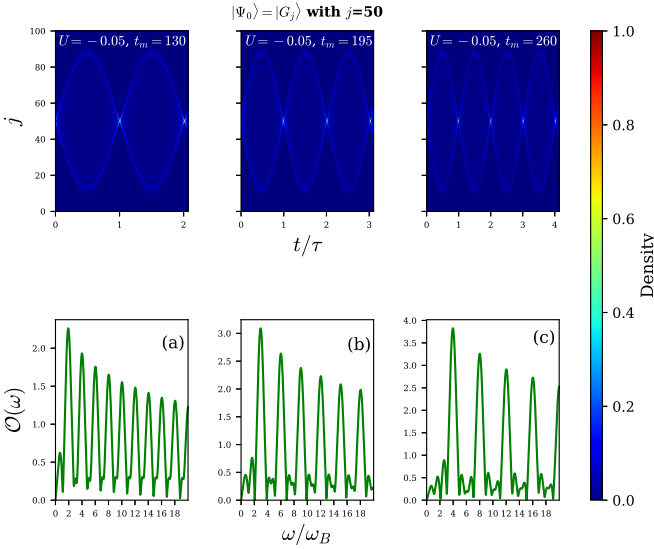


FIG. 6. The evolution of particle density at critical on-site interaction $U = -F/2$ starting from the ground state $|G_j\rangle$, with $j = 50$, and the associated $\mathcal{O}(\omega)$. The maximal evolution times are respectively $t_m = 130, 195$, and 260 .

expressed as

$$\left(\frac{\Delta F}{F}\right)_{U=0} = \frac{\hbar}{2\sqrt{6}Jt}, \quad (8)$$

for ultracold atoms with kinetic energy as low as 1 nK, where $J \sim k_B T \approx 1.38 \times 10^{-32}$ J. At $t = 130$, $(\Delta F/F)_{U=0} = 1.20 \times 10^{-5}$ or 12 parts per million (ppm), approximately half of the 22 ppm relative standard uncertainty recommended by the Committee on Data for Science and Technology [64]. The rate of the two uncertainties is

$$\frac{(\Delta F/F)_{\min}}{(\Delta F/F)_{U=0}} = \frac{2\sqrt{2}\hbar}{dFt} \approx 2.43 \times 10^{-6}, \quad (9)$$

considering $t = 130$, $d = 680$ nm, and $F = mg \approx 1.39 \times 10^{-24}$ N for a Rb atom.

In Fig. 6, the evolution of particle density at the critical value $U = -0.05$ and the corresponding $\mathcal{O}(\omega)$ are illustrated. Interestingly, Figs. 6(a), 6(b), and 6(c) display peak coordinates around $\omega/\omega_B = [2, 4, 6, \dots, 18]$, $[3, 6, 9, \dots, 18]$, and $[4, 8, 12, 16]$, respectively. Figure 6(a) reveals peak coordinates divided by 2, 4, 6, ..., 18, respectively, then subtracted by 1, yielding $[-0.0360, 0.000750, 0.00400, \dots]$. The root mean square of these data gives $(\Delta\omega_B/\omega_B)_0 \approx 1.24 \times 10^{-2}$. Given $\hbar\omega_B = Fd$, the bare uncertainty $(\Delta F/F)_0 = (\Delta\omega_B/\omega_B)_0$. Similarly, Figs. 6(b) and 6(c) provide $(\Delta\omega_B/\omega_B)_0 \approx 7.46 \times 10^{-3}$ and 5.29×10^{-3} , respectively. These results depend on the step size and range of ω , as well as the evolution of particle density.

The remarkable progress in precision measurement is exemplified by the study of interacting bosons with tailored on-site interactions. However, the significance of this proposal extends beyond its immediate scope. Utilizing neutral bosonic atoms, such as Rb, as a prime example, we consider a scenario where three atoms, each separated by a distance a within a

one-dimensional lattice, are confined to a single site, with a significantly smaller than the lattice spacing d ($a \ll d$). The Casimir energy between each pair of atoms separated by a distance a is determined by the expression

$$E_c(a) = -\frac{23}{4\pi}\hbar c \frac{\alpha_1\alpha_2}{a^7}, \quad (10)$$

where α_1 and α_2 represent the static polarizabilities of the atoms [83,84]. Taking $\alpha_1 = \alpha_2 = 4\pi r^3/3$, with the atom radius $r = 265$ pm, and $d = 100a$, we apply the criterion $|E_c(a)| = Fd/2$ to determine $a \approx 38.7$ nm, surpassing the atom radius r . Consequently, the Casimir energy and the Casimir-Polder force are approximately $E_c(a) \approx -2.69 \times 10^{-30}$ J and $F_c(a) \approx -4.87 \times 10^{-22}$ N, respectively, with $F_c(a)$ exceeding the weight of a Rb atom by 2 orders of magnitude.

To realize the critical value criterion, one can adjust the lattice spacing d and measure the bare uncertainties at a fixed maximal evolution time. Once the bare uncertainty reaches a minimum, the criterion is achieved. By fixing the lattice spacing d and increasing the value of a , the Casimir energy diminishes rapidly. Injecting energy equivalent to $(Fd/2 - |E_c(a)|)$ into the trapped particles allows the critical value criterion to be met. Subsequent accurate counting of the injected energy enables the measurement of the Casimir energy and the Casimir-Polder force. For precise measurement of the Casimir-Polder force, a preferable scenario involves a two-boson system occupying adjacent sites in a two-dimensional lattice, although this is not discussed here.

In the preceding illustrative calculations, the kinetic energy of an ultracold atom at 1 nK is approximately 10^{-32} J, significantly smaller than the estimated Casimir energy at around 10^{-30} J. Consequently, the noise originating from the ultracold atoms can be effectively mitigated. However, as the proposed approach remains theoretical at this stage, definitive knowledge concerning potential imperfections is currently lacking.

It might be noticed that there are some similarities between the three-boson model with only on-site interaction and the three-fermion model with nearest-neighbor interaction. This raises the question of whether there are similarities in the QFI of the two models. In Fig. 7, QFI values (Q) are depicted over time for the two models with different interaction strengths. When the interactions are weak, the Q value of the three-fermion model approaches that of a single-particle model as the interaction strengths decrease, while the Q value of the three-boson model triples. When the interactions are strong, the Q values of both models decrease rapidly with increasing interaction strengths, with the three-boson model's Q value decreasing slightly more quickly. At moderate interaction strengths $U = V = 0.07$, the Q values of both models reach considerable magnitudes over time. As expected, there are critical values of $V = \pm F$ at which the Q value reaches the maximum $J^2 t^4$, which is one-third of the maximum Q value of the three-boson model with only on-site interaction. Since the quartic curves themselves are trivial, we do not include them in the figure. Because the Casimir-Polder force between neutral atoms is sensitive to their spacing, a three-fermion prototype with only nearest-neighbor interaction would face a dilemma: measuring the Casimir-Polder force

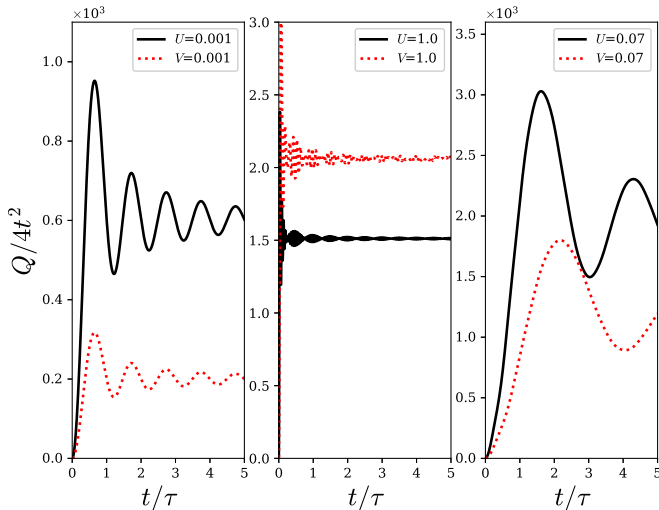


FIG. 7. The depicted QFI values (Q) in terms of $4t^2$ vary with time t/τ for the three-boson model with only on-site interaction U and the three-fermion model with only nearest-neighbor interaction V . The initial states for the two models are three bosons sitting on a single site and three fermions sitting on three sequential sites, respectively. The interaction strengths are chosen as weak $U = V = 0.001$, strong $U = V = 1.0$, and moderate $U = V = 0.07$. Q is symmetric with respect to the signs of the interactions.

with fixed lattice spacing and adjusting the lattice spacing to meet some critical value criterion. Furthermore, when three neutral fermionic atoms with only nearest-neighbor interactions are arranged in a line, the Casimir-Polder force between the first and third atoms becomes significant. In such cases, it is essential to include next-nearest-neighbor interactions in the three-fermion model to accurately describe the system.

VI. CONCLUSION

Examining the energy spectrum of the one-dimensional three-boson system with on-site interaction unveils that the energy band structure is predominantly shaped by the contri-

bution of one or two particles within the system. In contrast, the emergence of the energy level structure stems from the collective behavior of the entire system, where three particles are intricately bound together. Intriguingly, the three-boson system with on-site interaction showcases clustering behavior akin to that of the three-fermion system with nearest-neighbor interactions. This observation suggests the effective substitutability of the boson system for a fermion system in specific scenarios. Unlike other three-particle systems with strong interactions that yield multiple-frequency information, our model distinctly provides a characteristic frequency for the bulk system.

At specific values of on-site interaction (i.e., $U = \pm Fd/2$), the QFI exhibits a remarkable proportionality to t^4 , a phenomenon not observed before in other two- or three-particle systems. This unique behavior implies that the relative uncertainty in measuring big G or the Eötvös parameter can be as low as 2.4 ppm of the relative uncertainties in the absence of on-site interactions, provided that all other related observables can be measured with enough precision. In the proposed experimental framework, meticulously tailored for neutral bosonic atom systems, conducting measurements for the Casimir energy is entirely feasible. This endeavor promises to unveil a captivating connection between the Casimir-Polder force and gravity. Both refining the measurement precision of the Newtonian gravitational constant and measuring the Casimir-Polder force between neutral particles deserve experimentalists dedicating a significant amount of time and effort to bring them to fruition. Our proposed scheme offers the opportunity to address both tasks concurrently.

Leveraging cutting-edge facilities and techniques such as periodic optical lattices [85], magneto-optic traps [86], and gravimeters or quantum gravity gradiometers [87], we anticipate the actualization of the proposed experiments in the near future.

ACKNOWLEDGMENTS

One of the authors (H.Y.) would like to express gratitude to Prof. X. Guan for valuable comments on this project.

- [1] Y. Aharonov, L. Davidovich, and N. Zagury, Quantum random walks, *Phys. Rev. A* **48**, 1687 (1993).
- [2] J. Kempe, Quantum random walks: An introductory overview, *Contemp. Phys.* **44**, 307 (2003).
- [3] A. Ambainis, Quantum walks and their algorithmic applications, *Int. J. Quantum Inf.* **01**, 507 (2003).
- [4] J. Du, H. Li, X. Xu, M. Shi, J. Wu, X. Zhou, and R. Han, Experimental implementation of the quantum random-walk algorithm, *Phys. Rev. A* **67**, 042316 (2003).
- [5] B. Yang, H. Sun, R. Ott, H.-Y. Wang, T. V. Zache, J. C. Halimeh, Z.-S. Yuan, P. Hauke, and J.-W. Pan, Observation of gauge invariance in a 71-site Bose-Hubbard quantum simulator, *Nature (London)* **587**, 392 (2020).
- [6] H. Sun, B. Yang, H.-Y. Wang, Z. Y. Zhou, G.-X. Su, H.-N. Dai, Z.-S. Yuan, and J.-W. Pan, Realization of a bosonic antiferromagnet, *Nat. Phys.* **17**, 990 (2021).
- [7] P. Scholl, A. L. Shaw, R. B.-S. Tsai, R. Finkelstein, J. Choi, and M. Endres, Erasure conversion in a high-fidelity Rydberg quantum simulator, *Nature (London)* **622**, 273 (2023).
- [8] S. Ma, G. Liu, P. Peng, B. Zhang, S. Jandura, J. Claes, A. P. Burgers, G. Pupillo, S. Puri, and J. D. Thompson, High-fidelity gates and mid-circuit erasure conversion in an atomic qubit, *Nature (London)* **622**, 279 (2023).
- [9] S. E. Venegas-Andraca, Quantum walks: A comprehensive review, *Quantum Inf. Process.* **11**, 1015 (2012).
- [10] F. Zatelli, C. Benedetti, and M. G. A. Paris, Scattering as a quantum metrology problem: A quantum walk approach, *Entropy* **22**, 1321 (2020).
- [11] A. M. Childs, D. Gosset, and Z. Webb, Universal computation by multiparticle quantum walk, *Science* **339**, 791 (2013).
- [12] S. Lloyd, Quantum coherence in biological systems, *J. Phys.: Conf. Ser.* **302**, 012037 (2011).

- [13] A. Bisio, G. M. D'Ariano, P. Perinotti, and A. Tosini, Thirring quantum cellular automaton, *Phys. Rev. A* **97**, 032132 (2018).
- [14] I. Vakulchyk, M. V. Fistul, P. Qin, and S. Flach, Anderson localization in generalized discrete-time quantum walks, *Phys. Rev. B* **96**, 144204 (2017).
- [15] J. K. Asbóth, Symmetries, topological phases, and bound states in the one-dimensional quantum walk, *Phys. Rev. B* **86**, 195414 (2012).
- [16] T. Kitagawa, M. A. Broome, A. Fedrizzi, M. S. Rudner, E. Berg, I. Kassal, A. Aspuru-Guzik, E. Demler, and A. G. White, Observation of topologically protected bound states in photonic quantum walks, *Nat. Commun.* **3**, 882 (2012).
- [17] Y. E. Kraus, Y. Lahini, Z. Ringel, M. Verbin, and O. Zilberberg, Topological states and adiabatic pumping in quasicrystals, *Phys. Rev. Lett.* **109**, 106402 (2012).
- [18] M. Verbin, O. Zilberberg, Y. E. Kraus, Y. Lahini, and Y. Silberberg, Observation of topological phase transitions in photonic quasicrystals, *Phys. Rev. Lett.* **110**, 076403 (2013).
- [19] M. Atala, M. Aidelsburger, J. T. Barreiro, D. Abanin, T. Kitagawa, E. Demler, and I. Bloch, Direct measurement of the Zak phase in topological Bloch bands, *Nat. Phys.* **9**, 795 (2013).
- [20] V. V. Ramasesh, E. Flurin, M. Rudner, I. Siddiqi, and N. Y. Yao, Direct probe of topological invariants using Bloch oscillating quantum walks, *Phys. Rev. Lett.* **118**, 130501 (2017).
- [21] A. Ahlbrecht, A. Alberti, D. Meschede, V. B. Scholz, A. H. Werner, and R. F. Werner, Molecular binding in interacting quantum walks, *New J. Phys.* **14**, 073050 (2012).
- [22] T. Fukuhara, P. Schauß, M. Endres, S. Hild, M. Cheneau, I. Bloch, and C. Gross, Microscopic observation of magnon bound states and their dynamics, *Nature (London)* **502**, 76 (2013).
- [23] H. Zhang, Y. Zhai, and X. Chen, Spin dynamics in one-dimensional optical lattices, *J. Phys. B* **47**, 025301 (2014).
- [24] W. Liu, Y. Ke, L. Zhang, and C. Lee, Bloch oscillations of multimagnon excitations in a Heisenberg XXZ chain, *Phys. Rev. A* **99**, 063614 (2019).
- [25] M. Karski, L. Förster, J.-M. Choi, A. Steffen, W. Alt, D. Meschede, and A. Widera, Quantum walk in position space with single optically trapped atoms, *Science* **325**, 174 (2009).
- [26] T. Fukuhara, A. Kantian, M. Endres, M. Cheneau, P. Schauß, S. Hild, D. Bellem, U. Schollwöck, T. Giamarchi, C. Gross, I. Bloch, and S. Kuhr, Quantum dynamics of a mobile spin impurity, *Nat. Phys.* **9**, 235 (2013).
- [27] A. W. Young, W. J. Eckner, N. Schine, A. M. Childs, and A. M. Kaufman, Tweezer-programmable 2D quantum walks in a Hubbard-regime lattice, *Science* **377**, 885 (2022).
- [28] H. Schmitz, R. Matjeschk, C. Schneider, J. Glueckert, M. Enderlein, T. Huber, and T. Schaetz, Quantum walk of a trapped ion in phase space, *Phys. Rev. Lett.* **103**, 090504 (2009).
- [29] F. Zähringer, G. Kirchmair, R. Gerritsma, E. Solano, R. Blatt, and C. F. Roos, Realization of a quantum walk with one and two trapped ions, *Phys. Rev. Lett.* **104**, 100503 (2010).
- [30] A. Schreiber, K. N. Cassemiro, V. Potoček, A. Gábris, I. Jex, and C. Silberhorn, Decoherence and disorder in quantum walks: from ballistic spread to localization, *Phys. Rev. Lett.* **106**, 180403 (2011).
- [31] R. H. Brown and R. Q. Twiss, Correlation between photons in two coherent beams of light, *Nature (London)* **177**, 27 (1956).
- [32] M. Hillery, Quantum walks through a waveguide maze, *Science* **329**, 1477 (2010).
- [33] A. Peruzzo, M. Lobino, J. C. F. Matthews, N. Matsuda, A. Politi, K. Poulios, X. Zhou, Y. Lahini, N. Ismail, K. Wörhoff, Y. Bromberg, Y. Silberberg, M. G. Thompson, and J. L. O'Brien, Quantum walks of correlated photons, *Science* **329**, 1500 (2010).
- [34] A. Schreiber, K. N. Cassemiro, V. Potoček, A. Gábris, P. J. Mosley, E. Andersson, I. Jex, and C. Silberhorn, Photons walking the line: A quantum walk with adjustable coin operations, *Phys. Rev. Lett.* **104**, 050502 (2010).
- [35] M. A. Broome, A. Fedrizzi, B. P. Lanyon, I. Kassal, A. Aspuru-Guzik, and A. G. White, Discrete single-photon quantum walks with tunable decoherence, *Phys. Rev. Lett.* **104**, 153602 (2010).
- [36] A. S. Solntsev, A. A. Sukhorukov, D. N. Neshev, and Y. S. Kivshar, Spontaneous parametric down-conversion and quantum walks in arrays of quadratic nonlinear waveguides, *Phys. Rev. Lett.* **108**, 023601 (2012).
- [37] M. Tamura, T. Mukaiyama, and K. Toyoda, Quantum walks of a phonon in trapped ions, *Phys. Rev. Lett.* **124**, 200501 (2020).
- [38] Y. Omar, N. Paunković, L. Sheridan, and S. Bose, Quantum walk on a line with two entangled particles, *Phys. Rev. A* **74**, 042304 (2006).
- [39] R. Khomeriki, D. O. Krimer, M. Haque, and S. Flach, Interaction-induced fractional Bloch and tunneling oscillations, *Phys. Rev. A* **81**, 065601 (2010).
- [40] K. Mayer, M. C. Tichy, F. Mintert, T. Konrad, and A. Buchleitner, Counting statistics of many-particle quantum walks, *Phys. Rev. A* **83**, 062307 (2011).
- [41] L. Sansoni, F. Sciarrino, G. Vallone, P. Mataloni, A. Crespi, R. Ramponi, and R. Osellame, Two-particle bosonic-fermionic quantum walk via integrated photonics, *Phys. Rev. Lett.* **108**, 010502 (2012).
- [42] Y. Lahini, M. Verbin, S. D. Huber, Y. Bromberg, R. Pugatch, and Y. Silberberg, Quantum walk of two interacting bosons, *Phys. Rev. A* **86**, 011603(R) (2012).
- [43] C. Benedetti, F. Buscemi, and P. Bordone, Quantum correlations in continuous-time quantum walks of two indistinguishable particles, *Phys. Rev. A* **85**, 042314 (2012).
- [44] G. Corrielli, A. Crespi, G. Della Valle, S. Longhi, and R. Osellame, Fractional Bloch oscillations in photonic lattices, *Nat. Commun.* **4**, 1555 (2013).
- [45] X. Qin, Y. Ke, X. Guan, Z. Li, N. Andrei, and C. Lee, Statistics-dependent quantum co-walking of two particles in one-dimensional lattices with nearest-neighbor interactions, *Phys. Rev. A* **90**, 062301 (2014).
- [46] P. L. Krapivsky, J. M. Luck, and K. Mallick, Interacting quantum walkers: Two-body bosonic and fermionic bound states, *J. Phys. A* **48**, 475301 (2015).
- [47] I. Siloi, C. Benedetti, E. Piccinini, J. Piilo, S. Maniscalco, M. G. A. Paris, and P. Bordone, Noisy quantum walks of two indistinguishable interacting particles, *Phys. Rev. A* **95**, 022106 (2017).
- [48] D. Wiater, T. Sowiński, and J. Zakrzewski, Two bosonic quantum walkers in one-dimensional optical lattices, *Phys. Rev. A* **96**, 043629 (2017).

- [49] A. Beggi, I. Siloi, C. Benedetti, E. Piccinini, L. Razzoli, P. Bordone, and M. G. A. Paris, Back and forth from Fock space to Hilbert space: a guide for commutators, *Eur. J. Phys.* **39**, 065401 (2018).
- [50] S. Sarkar and T. Sowiński, Correlations in few two-component quantum walkers on a tilted lattice, *Phys. Rev. A* **102**, 043326 (2020).
- [51] L. Wang, L. Wang, and Y. Zhang, Quantum walks of two interacting anyons in one-dimensional optical lattices, *Phys. Rev. A* **90**, 063618 (2014).
- [52] W. S. Dias, E. M. Nascimento, M. L. Lyra, and F. A. B. F. de Moura, Frequency doubling of Bloch oscillations for interacting electrons in a static electric field, *Phys. Rev. B* **76**, 155124 (2007).
- [53] Y. A. Kosevich and V. V. Gann, Magnon localization and Bloch oscillations in finite Heisenberg spin chains in an inhomogeneous magnetic field, *J. Phys.: Condens. Matter* **25**, 246002 (2013).
- [54] C. Cedzich, T. Rybár, A. H. Werner, A. Alberti, M. Genske, and R. F. Werner, Propagation of quantum walks in electric fields, *Phys. Rev. Lett.* **111**, 160601 (2013).
- [55] P. Arnault, B. Pepper, and A. Pérez, Quantum walks in weak electric fields and Bloch oscillations, *Phys. Rev. A* **101**, 062324 (2020).
- [56] I. Carusotto, L. Pitaevskii, S. Stringari, G. Modugno, and M. Inguscio, Sensitive measurement of forces at the micron scale using Bloch oscillations of ultracold atoms, *Phys. Rev. Lett.* **95**, 093202 (2005).
- [57] G. Ferrari, N. Poli, F. Sorrentino, and G. M. Tino, Long-lived Bloch oscillations with bosonic Sr atoms and application to gravity measurement at the micrometer scale, *Phys. Rev. Lett.* **97**, 060402 (2006).
- [58] M. G. Tarallo, T. Mazzoni, N. Poli, D. V. Sutyryn, X. Zhang, and G. M. Tino, Test of Einstein equivalence principle for 0-spin and half-integer-spin atoms: Search for spin-gravity coupling effects, *Phys. Rev. Lett.* **113**, 023005 (2014).
- [59] Z. A. Geiger, K. M. Fujiwara, K. Singh, R. Senaratne, S. V. Rajagopal, M. Lipatov, T. Shimasaki, R. Driben, V. V. Konotop, T. Meier, and D. M. Weld, Observation and uses of position-space Bloch oscillations in an ultracold gas, *Phys. Rev. Lett.* **120**, 213201 (2018).
- [60] C. W. Helstrom, *Quantum Detection and Estimation Theory* (Academic, New York, 1976).
- [61] L. Pezzè, A. Smerzi, M. K. Oberthaler, R. Schmied, and P. Treutlein, Quantum metrology with nonclassical states of atomic ensembles, *Rev. Mod. Phys.* **90**, 035005 (2018).
- [62] J. Liu, H. Yuan, X.-M. Lu, and X. Wang, Quantum Fisher information matrix and multiparameter estimation, *J. Phys. A* **53**, 023001 (2020).
- [63] P. Asenbaum, C. Overstreet, M. Kim, J. Curti, and M. A. Kasevich, Atom-interferometric test of the equivalence principle at the 10^{-12} level, *Phys. Rev. Lett.* **125**, 191101 (2020).
- [64] E. Tiesinga, P. J. Mohr, D. B. Newell, and B. N. Taylor, CODATA recommended values of the fundamental physical constants: 2018, *Rev. Mod. Phys.* **93**, 025010 (2021).
- [65] P. M. Preiss, R. Ma, M. E. Tai, A. Lukin, M. Rispoli, P. Zupancic, Y. Lahini, R. Islam, and M. Greiner, Strongly correlated quantum walks in optical lattices, *Science* **347**, 1229 (2015).
- [66] X. Cai, H. Yang, H.-L. Shi, C. Lee, N. Andrei, and X.-W. Guan, Multiparticle quantum walks and Fisher information in one-dimensional lattices, *Phys. Rev. Lett.* **127**, 100406 (2021).
- [67] H.-M. Li and G.-M. Zeng, Quantum walks of three interacting bosons on one-dimensional optical lattices, *Quantum Inf. Process.* **20**, 266 (2021).
- [68] S. Paeckel, T. Köhler, A. Swoboda, S. R. Manmana, U. Schollwöck, and C. Hubig, Time-evolution methods for matrix-product states, *Ann. Phys.* **411**, 167998 (2019).
- [69] G. Vidal, Efficient classical simulation of slightly entangled quantum computations, *Phys. Rev. Lett.* **91**, 147902 (2003); Efficient simulation of one-dimensional quantum many-body systems, **93**, 040502 (2004).
- [70] M. Zwolek and G. Vidal, Mixed-state dynamics in one-dimensional quantum lattice systems: A time-dependent super-operator renormalization algorithm, *Phys. Rev. Lett.* **93**, 207205 (2004).
- [71] F. Verstraete, J. J. García-Ripoll, and J. I. Cirac, Matrix product density operators: Simulation of finite-temperature and dissipative systems, *Phys. Rev. Lett.* **93**, 207204 (2004).
- [72] S. R. White and A. E. Feiguin, Real-time evolution using the density matrix renormalization group, *Phys. Rev. Lett.* **93**, 076401 (2004).
- [73] A. J. Daley, C. Kollath, U. Schollwöck, and G. Vidal, Time-dependent density-matrix renormalization-group using adaptive effective Hilbert spaces, *J. Stat. Mech.* (2004) P04005.
- [74] M. P. Zaletel, R. S. K. Mong, C. Karrasch, J. E. Moore, and F. Pollmann, Time-evolving a matrix product state with long-ranged interactions, *Phys. Rev. B* **91**, 165112 (2015).
- [75] M. L. Wall and L. D. Carr, Out-of-equilibrium dynamics with matrix product states, *New J. Phys.* **14**, 125015 (2012).
- [76] P. E. Dargel, A. Wöllert, A. Honecker, I. P. McCulloch, U. Schollwöck, and T. Pruschke, Lanczos algorithm with matrix product states for dynamical correlation functions, *Phys. Rev. B* **85**, 205119 (2012).
- [77] D. Jaschke, M. L. Wall, and L. D. Carr, Open source matrix product states: Opening ways to simulate entangled many-body quantum systems in one dimension, *Comput. Phys. Commun.* **225**, 59 (2018).
- [78] J. Haegeman, J. I. Cirac, T. J. Osborne, I. Pižorn, H. Verschelde, and F. Verstraete, Time-dependent variational principle for quantum lattices, *Phys. Rev. Lett.* **107**, 070601 (2011).
- [79] J. Haegeman, C. Lubich, I. Oseledets, B. Vandereycken, and F. Verstraete, Unifying time evolution and optimization with matrix product states, *Phys. Rev. B* **94**, 165116 (2016).
- [80] F. W. Strauch, Connecting the discrete- and continuous-time quantum walks, *Phys. Rev. A* **74**, 030301(R) (2006).
- [81] M. Takahashi, Half-filled Hubbard model at low temperature, *J. Phys. C* **10**, 1289 (1977).
- [82] J. Yu, N. Sun, and H. Zhai, Symmetry protected dynamical symmetry in the generalized Hubbard models, *Phys. Rev. Lett.* **119**, 225302 (2017).
- [83] H. B. G. Casimir and D. Polder, The influence of retardation on the London-van der Waals forces, *Phys. Rev.* **73**, 360 (1948).
- [84] H. B. G. Casimir, On the attraction between two perfectly conducting plates, *Proc. K. Ned. Akad. Wet.* **51**, 793 (1948).

- [85] M. H. Anderson, J. R. Ensher, M. R. Matthews, C. E. Wieman, and E. A. Cornell, Observation of Bose-Einstein condensation in a dilute atomic vapor, [Science](#) **269**, 198 (1995).
- [86] J. Dalibard and C. Cohen-Tannoudji, Laser cooling below the Doppler limit by polarization gradients: Simple theoretical models, [J. Opt. Soc. Am. B](#) **6**, 2023 (1989).
- [87] B. Stray, A. Lamb, A. Kaushik, J. Vovrosh, A. Rodgers, J. Winch, F. Hayati, D. Boddice, A. Stabrawa, A. Niggebaum, M. Langlois, Yu.-H. Lien, S. Lellouch, S. Roshanmanesh, K. Ridley, G. de Villiers, G. Brown, T. Cross, G. Tuckwell, A. Faramarzi *et al.*, Quantum sensing for gravity cartography, [Nature \(London\)](#) **602**, 590 (2022).